EUROPEAN ORGANIZATION FOR NUCLEAR RESEARCH

CERN-SL-2001-012 AP
CLIC Note 477

Heat deposition by transient beam passage in spoilers

S. Fartoukh, J.B. Jeanneret and J. Pancin

Abstract

Future electron-positron linear colliders must produce bunches of tiny emittance grouped in short bunch trains in order to provide adequately large luminosities. A collimation system must be installed between the end of the main linac and the optical elements of the final focus to protect the detectors from errant beams. With ordinary values of the betatron functions, the transverse beam size is of a few microns. With such sizes, the local deposition of heat of even a single bunch train is so high that no material can survive such an event. The problem is solved by increasing the beam sizes at the location of the collimators. But the use of large betatron functions is costly and can induce strong optical errors. It is therefore important to compute precisely safe beam sizes which allow the survival of the collimators, in order to limit their increase to the minimum needed. The deposition of heat occurs both by ionisation along the path of the particles which traverse the material and by ohmic image current heating at the surface of the collimator, for that fraction of the beam which flies outside the collimator. With small bunches, heat diffusion is substantial even with short bunch trains and helps to reduce the excursion of temperature. The rise of temperature is computed by solving analytically the time-dependent heat equation in two spatial dimensions near an interface with vacuum. Numerical results are given for the CLIC study.

Paper submitted to Physical Review ST-AB

Geneva, Switzerland

March 2001

1 Introduction

In future linear colliders, which shall provide beams of tiny transverse sizes in the TeV range, a collimation system must be installed upstream of the experiments, to protect them both from beam halo and from errant beams which can be destructive for either the final focus optical system or the parts of the detector which are located near the beam axis. The beam sizes are so small that heat deposition is of paramount importance in the design of the collimation system. Dumping a bunch train directly on a massive object is not doable even with the most suitable materials [1, 2, 3, 4]. The present solution to this difficulty is to increase the size of the errant beam by using a thin piece of material, called 'spoiler' below, which is short enough to avoid particle multiplication by hard electromagnetic interactions. The spoiler shall be located at a position where the beam sizes are large enough to avoid an excessive rise of temperature. Then, at a suitable distance downstream of the spoiler, where the scattered beam is large enough, a massive dump can absorb it safely. In this paper, we restrict our study to heat issues in order to specify the conditions under which a spoiler can survive to the traversal of a full bunch train in the worst possible condition. We also restrict our study to spoilers made of conducting materials. The case of insulators will be briefly evoked. The case of conducting spoilers was studied recently by X.E. Lin and D.H. Whittum [5]. The authors identified the two major contributions to heat deposition, namely ionisation and image current ohmic heating. We make full use of their treatment of the image current, but work out the diffusion of heat in a more detailed way. We use Green functions to solve analytically the time-dependent heat equation in two dimensions, for the sum of the ionisation and image current contributions, without approximations, except for one harmless exception, and without restrictions about the beam parameters. We express our results with integrals of a single variable, which are computed numerically with fast algorithms. In Section 2, we describe the problem that we propose to solve. The properties of a set of materials are presented in Section 3 while the processes which deposit heat in the spoiler are described in Section 4. We outline the way of solving the heat equation in Section 5, while the full derivation can be found in Appendices A, B and C. In Section 6, we treat numerically the case of the bunch trains of the CLIC study [3]. Finally in Section 7, we briefly discuss the case of dielectric spoilers.

2 Description of the problem

In a coordinate system where x and y are respectively the horizontal and vertical transverse axis and z is the longitudinal one, the spoiler occupies the half-infinite space $y \geq 0$. The plane $y = 0$ will be called septum in the following. In practice, the length of the spoiler will be limited to $\Delta z \approx 0.5 L_R$, with L_R the electro-

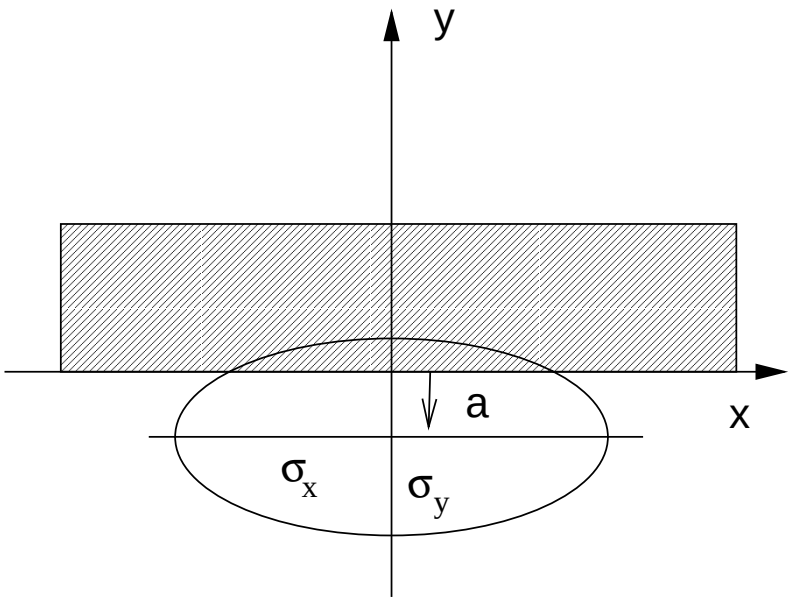

Figure 1: A bunch of horizontal and vertical r.m.s. beam sizes σ_x and σ_y impacting on a spoiler. The quantity $y = a$ is the distance between the centre of the beam and the edge of the collimator. The case shown has $a < 0$. If $|a| \gg \sigma_y$ and $a < 0$, the beam is outside the spoiler. If $|a| \gg \sigma_y$ and $a > 0$, the beam fully impacts the spoiler.

magnetic radiation length, see Table 1. The quantity L_R is much larger than the transverse beam sizes. The beam centroid travels along a line parallel to z defined by $(x = 0, y = a)$, as shown in Fig. 1. The quantity a is called below the impact parameter. The beam consists of bunch trains. Each train consists of $N + 1$ bunches of r.m.s bunch length $\sigma_z = c\,\sigma_t$. The bunches are separated by $\delta_z = c\delta_t$ and the time elapsed during the passage of a train is $\Delta t = N\delta_t$. The distance between trains is large and we do not consider the residual heat deposited by former trains. Once an errant beam has touched a spoiler, the status of the machine must be checked and readjusted before a full new train is injected, thus leaving enough time for the spoiler to cool down. The transverse density of electrons is a decoupled Gaussian distribution and writes

$$\frac{d^2n}{dx\,dy} = N_e\,\rho(x,y) = \frac{N_e}{2\pi\,\sigma_x\,\sigma_y}\,\exp\left(-\frac{x^2}{2\sigma_x^2} - \frac{(y-a)^2}{2\sigma_y^2}\right)\ , \tag{1}$$

with N_e the bunch population, σ_x and σ_y the transverse r.m.s beam sizes and the density function ρ normalised to

$$\int_{-\infty}^{+\infty} dx \int_{-\infty}^{+\infty} dy\ \rho(x,y) = 1\ . \tag{2}$$

The corresponding transverse distribution of charge is

$$q(x,y) = e\,N_e\,\rho(x,y) = Q\,\rho(x,y)\ , \tag{3}$$

with $Q = e\,N_e$ the bunch charge and e the elementary charge. For a given train structure, bunch population and spoiler characteristics, the map of temperature at the end of the train depends on three quantities, namely σ_x, σ_y and a, in addition to the data related to the spoiler itself. While σ_x and σ_y can be freely chosen, the impact parameter a cannot be controlled. The errant beam which must be intercepted by the spoiler can impact deeply onto its front face ($a \gg \sigma_y$), in which case the temperature rise is dominated by ionisation (See Section 4.1). If $-a > \sigma_y$, the image current ohmic heating described in Section 4.2 dominates, while in the case of an impact in the vicinity of the septum ($|a| \lesssim \sigma_y$) the two processes approximately add. For a given material, our aim is to compute a safe area in the plane (σ_x, σ_y) in which the spoiler will not be damaged whatever the value of a (see Section 3). The criterion for a safe condition is expressed by saying that the maximum of the temperature map at the end of the passage of a train is smaller than an upper limit T_l at any location in the spoiler, or

$$T_{\max} = \max_{(x,y)}\,[\,\Delta T(x,y,t = N\delta_t) + T_{\text{room}}\,]\ <\ T_l\ . \tag{4}$$

In practice, we fix σ_x and σ_y , then compute a temperature map for several values of a, in order to find which value of a maximises $T_{\max}$. While the condition (4) is not fulfilled , the procedure is iterated for a different value of σ_y. The whole process is repeated for different values of σ_x. We thus get a curve in the plane (σ_x, σ_y) above which the condition (4) is always met. The core of our work is the computation of the map of temperature at the end of a bunch train. We first assume that the heat diffusion length $d_b \stackrel{\text{def}}{=} \sqrt{2\,D\,\sigma_t}$ (corresponding to the bunch duration σ_t and the thermal diffusivity D of the material) is short compared to the smallest characteristic distance associated to heat deposition, which is the skin depth $\delta(\omega_z)$ (Eq. 9) of the image current in our problem, see Section 3 and Table 4. It can be verified in Table 4 that this condition is largely met for the CLIC nominal bunch duration. Therefore, the initial deposition of heat occurs in a nearly adiabatic condition. On the other hand, the numbers in Table 4 indicate that the diffusion length over the duration Δt of the train, $d_{\text{train}} \stackrel{\text{def}}{=} \sqrt{2\,D\,\Delta t}$, is larger or of the same order of magnitude as $\delta(\omega_z)$. The heat will therefore substantially diffuse in the material and every bunch must be considered separately. This is obviously the case for the heat deposition by image current but even in the case of ionisation, if one of the transverse sizes of the beam is small enough, or $\sigma_{x,y} < d_{\text{train}} \lesssim 5\ \mu$m, the contribution of diffusion is no more negligible. We therefore treat the diffusion of heat without limiting approximations for both ionisation and image current.

In view of the large number of maps which must be computed, we solved the heat equation analytically. The results are either algebraic expressions or single

Table 1: The material data at room temperature. dE/dz is the energy loss, ρ the density, c_v the specific heat, K the thermal conductivity, L_R the radiation length, σ the electrical conductivity and $T_{\rm melt}$ the melting point.

	dE/dz	ρ	c_v	K	L_R	σ	$T_{\rm melt}$
	$[\mathrm{Jm}^{-1}]$	$[\mathrm{gm}^{-3}]$	$[\mathrm{Jm}^{-3}K^{-1}]$	$[\mathrm{Jm}^{-1}K^{-1}\mathrm{s}^{-1}]$	[m]	$[\Omega^{-1}\mathrm{m}^{-1}]$	[°C]
Be	6.61×10^{-11}	1.84×10^{6}	1.94×10^{6}	1.59×10^{2}	0.353	1.67×10^{7}	1278
C	8.85×10^{-11}	2.26×10^{6}	1.67×10^{6}	0.24×10^{2}	0.188	7.27×10^{4}	3550
Al	9.77×10^{-11}	2.70×10^{6}	2.24×10^{6}	2.21×10^{2}	0.089	3.77×10^{7}	660
Ti	1.50×10^{-10}	4.54×10^{6}	2.13×10^{6}	0.2×10^{2}	0.036	2.0×10^{6}	1660
Cu	2.81×10^{-10}	8.96×10^{6}	3.29×10^{6}	3.93×10^{2}	0.014	6.0×10^{7}	1083
W	4.95×10^{-10}	19.3×10^{6}	2.39×10^{6}	2.0×10^{2}	0.0035	1.81×10^{7}	3410

variable definite integrals, which for faster numerical calculations are evaluated using Gauss-Legendre integration methods [7].

3 Material data

We considered only elementary and conducting materials. The elements listed in Table 1 are chosen for either their high melting point or their good electrical conductivity. The data at room temperature are taken either in [8] or [9] . The energy loss by ionisation dE/dz is briefly discussed in Section 4.1. The specific heat c_v, the electrical conductivity σ and the thermal conductivity K all vary substantially with the temperature T. In order to take these variations into account while keeping the linearity of the heat equation, we choose a maximum allowed temperature excursion ΔT_l, above which fatigue can occur in the spoiler (see Section 3.1) and compute the average quantities $\bar{c_v}$, $\bar{\sigma}$ and $\bar{K}$ between $T_{\rm room}$ and $T_l = T_{\rm room} + \Delta T_l$. The specific heat per unit volume of a solid material is given by the Debye formula

$$c_v(T) = \frac{9\, N_a\, k_B\, \rho}{A} \left(\frac{T}{\Theta_d}\right)^3 \int_0^{\Theta_d/T} dx\, \frac{x^4 e^x}{(e^x-1)^2}\ , \tag{5}$$

with $N_a = 6.02 \times 10^{23}$ mole^{-1} the Avogadro number, $k_B = 1.38 \times 10^{-23}$ JK^{-1} the Boltzmann constant, ρ the density, A the atomic mass and Θ_d the Debye temperature of the material, see Table 1. The Eq. (5) is integrated numerically and the average $\bar{c_v}$ is easily calculated by neglecting the small dependence of the density ρ with temperature (in the worst case, namely graphite, $\Delta\rho/\rho = 3\alpha\Delta T_l = 7 \times 10^{-3}$, using the variables and the data of Tables 2 and 3). The electrical conductivity $\sigma(T)$ is taken from [10] and the average quantity $\bar{\sigma}$ between $T_{\rm room}$ and $T_l = T_{\rm room} + \Delta T_l$ is computed. The thermal and electrical conductivities of

conductors are related by the Wiedemann-Franz law

$$K_{\mathrm{WF}}(T) = \frac{\pi^2}{2}\left(\frac{k_B}{e}\right)^2 \sigma(T)\, T \ , \tag{6}$$

with e the elementary electric charge. Comparing Eq. (6) and the data at room temperature in Table 1, we find relative departures ranging from 9% for copper to 40% for Ti. We therefore define our average value $\bar{K}$ with

$$\bar{K} \stackrel{\mathrm{def}}{=} \frac{1}{2}\left(1 + \frac{K_{\mathrm{WF}}(T_l)}{K_{\mathrm{WF}}(T_{\mathrm{room}})}\right) K_{\mathrm{room}} \, , \tag{7}$$

where K_{room} is the thermal conductivity measured at room temperature taken from [9]. We did not apply Eq. (7) to graphite which is a too poor conductor to obey the Wiedemann-Franz law. In addition, its electrical conductivity can vary in a quite large range [10]. We therefore use room temperature values for K and σ in this case, keeping in mind that the results obtained for graphite have a partly indicative value. The averaged quantities are given in Table 3. Finally we define the thermal diffusivity with

$$D \stackrel{\mathrm{def}}{=} \bar{K}/\bar{c_v} \ . \tag{8}$$

In Table 4, we give the skin depth $\delta(\omega_z)$ of the material computed at the characteristic frequency $\omega_z \stackrel{\mathrm{def}}{=} 1/\sigma_t$ of the bunch:

$$\delta(\omega_z) \stackrel{\mathrm{def}}{=} \sqrt{\frac{2}{\omega_z\, \mu_0\, \sigma}} = \sqrt{\frac{2\,\sigma_t}{\mu_0\, \sigma}} \, , \tag{9}$$

with σ_t the r.m.s. bunch duration (Table 5), $\mu_0 = 4\pi \times 10^{-7}$ NA^{-2} the permeability of free space, and σ the electrical conductivity of the material taken from Table 1. It must be noted that if the surface roughness of the spoiler is larger than the skin depth, the effective electrical conductivity will be smaller than the quoted values. For CLIC parameters, the skin depth ranges from $\delta(\omega_z) = 1.5\mu$m (graphite) to 0.1μm (beryllium and copper). The surface roughness shall be kept to a fraction of these numbers to minimise image current ohmic heating. It must also be remarked that the conductivity of metals in the THz domain is not well known while the characteristic frequency of CLIC bunches is $\nu_\sigma = 1/(2\pi\sigma_t) = 1.6$ THz. Some measurements [11] indicate that absorption losses are larger or equal to ohmic ones in this range of frequency. For further discussion, we also compute in Table 4 some diffusion lengths with the formula $d = (2Dt)^{1/2}$ associated to the characteristic time parameters of the CLIC bunch trains which are listed in Table 5.

Table 2: Mechanical data and two estimators for the allowed temperature excursion. Y is the Young modulus, α the coefficient of thermal expansion, σ_{uts} the ultimate tensile strength, ΔT_1 the empirical limit temperature defined by equation (10) and ΔT_2 the temperature corresponding to the ultimate tensile strength limit, see Section 3.1.

	Y [MPa]	α $[(^\circ K)^{-1}]$	$\sigma_{\rm uts}$ [MPa]	ΔT_1 $[^\circ K]$	ΔT_2 $[^\circ K]$
Be	2.6×10^5	12.4×10^{-6}	800	792	174
C	4.9×10^3	3×10^{-6}	400	2383	19000
Al	7×10^4	24×10^{-6}	450	360	187
Ti	1.2×10^5	8.5×10^{-6}	400	1060	274
Cu	1.2×10^5	2×10^{-5}	300	656	88
W	4.1×10^5	4×10^{-6}	350	2285	149

Table 3: Properties of Material averaged between the room temperature $T_{\rm room}$ and the allowed excursion $T_{\rm room} + \Delta T_l$. Θ_d is the Debye temperature, ΔT_l the allowed variation of temperature, $\bar{c_v}$ the mean specific heat, $\bar{K}$ the mean thermal conductivity and $\bar{\sigma}$ the mean electrical conductivity, see Sections 3 and 3.1.

	Θ_d [K]	ΔT_l [K]	$\bar{c_v}$ $[\mathrm{Jm^{-3}}K^{-1}]$	$\bar{K}$ $[\mathrm{Jm^{-1}}K^{-1}\mathrm{s^{-1}}]$	$\bar{\sigma}$ $[\Omega^{-1}\mathrm{m^{-1}}]$
Be	1440	174	2.63×10^6	1.38×10^2	2.15×10^7
C	1500	2383	3.15×10^6	0.24×10^2	7.27×10^4
Al	430	187	2.32×10^6	2.18×10^2	2.93×10^7
Ti	420	274	2.22×10^6	0.2×10^2	1.45×10^6
Cu	340	88	3.34×10^6	3.87×10^2	5.15×10^7
W	400	149	2.45×10^6	1.98×10^2	1.42×10^7

Table 4: Some diffusion lengths, computed over the r.m.s bunch duration (d_b), the inter bunch time ($d_{\rm gap}$) and for the train duration ($d_{\rm train}$), as taken for the CLIC parameters of Table 5. They are compared to the penetration depth $\delta(\omega_z)$ of the image current. All data in meter.

	d_b	$d_{\rm gap}$	$d_{\rm train}$	$\delta(\omega_z)$
Be	1.87×10^{-9}	1.53×10^{-7}	1.90×10^{-6}	9.54×10^{-8}
C	8.79×10^{-10}	7.17×10^{-8}	8.90×10^{-7}	1.48×10^{-6}
Al	3.05×10^{-9}	2.49×10^{-7}	3.09×10^{-6}	7.33×10^{-8}
Ti	9.96×10^{-10}	8.13×10^{-8}	1.01×10^{-6}	3.57×10^{-7}
Cu	3.19×10^{-9}	2.61×10^{-7}	3.24×10^{-6}	6.22×10^{-8}
W	2.52×10^{-9}	2.06×10^{-7}	2.56×10^{-6}	1.30×10^{-7}

3.1 Allowed temperature excursion

We considered two criteria for acceptable temperature excursions and chose the most severe one for each material. The first one, used as a first guess value in metallurgy, considers the degradation of the mechanical properties of a material at temperatures which are close to the melting point. If ΔT_1 is the maximum acceptable excursion, $T_{\rm room}$ the room temperature and $T_{\rm melt}$ the melting temperature expressed in Kelvin, the rule is

$$\Delta T_1 \stackrel{\rm def}{=} 0.7\, T_{\rm melt} - T_{\rm room}\ . \tag{10}$$

With the second criterion, the stress induced by thermal expansion is compared to the ultimate tensile strength $\sigma_{\rm uts}$, or

$$\Delta T_2 \stackrel{\rm def}{=} \frac{2\,\sigma_{\rm uts}}{\alpha\, Y}\ , \tag{11}$$

with α the thermal expansion coefficient, Y the Young modulus and an empirical factor 2. The data and the allowed temperature excursions are given in Table 2. The safe limit $\Delta T_l \stackrel{\rm def}{=} \min\left[\,\Delta T_1\,,\,\Delta T_2\right]$ is given in Table 3. The limits $\Delta T_{1,2}$ are indicative and shall be adjusted to the data of the actual choice of a material.

4 Energy deposition

In this Section, we discuss the adiabatic deposition of heat at the passage of a single bunch either by ionisation or image current ohmic heating and show that black body radiation can be neglected.

4.1 Ionisation

Electrons deposit energy along their track by ionisation according to the Bethe-Bloch formula [9]. We multiplied the tabulated values of minimum energy deposition dE/dz by 1.4 to take into account the relativistic rise associated to high energy electron beams[9]. With the adiabatic condition and for a Gaussian beam of transverse bunch sizes $\sigma_{x,y}$, the initial map of temperature writes

$$T_{\rm ion}(x,y,t=0) = \frac{dE/dz}{c_v}\,\rho(x,y) = T_{0,\rm ion}\,h_x^0(x)\,h_y^0(y)\ , \tag{12}$$

with $\rho(x,y)$ taken from Eq. (1),

$$T_{0,\rm ion} \stackrel{\rm def}{=} \frac{N_e \times dE/dz}{2\pi\, c_v\, \sigma_x\, \sigma_y}\ , \tag{13}$$

$$h_x^0(x) \stackrel{\rm def}{=} \exp\left(-\frac{x^2}{2\sigma_x^2}\right)\ \text{and} \tag{14}$$

$$h_y^0(y) \stackrel{\text{def}}{=} \exp\left(-\frac{(y-a)^2}{2\sigma_y^2}\right) \ . \tag{15}$$

4.2 Image current ohmic heating

We use the exact 2D-transverse distribution of the energy deposited by image current derived in [5] for a point-like bunch centred at (x_0, y_0), namely

$$e_d(x,y) = \frac{Z_0\, c}{2\pi}\, \frac{Q^2}{\pi^2\, \sigma_z^2}\, f^2(x; x_0, y_0)\, g\big(y/\delta(\omega_z)\big) \ , \tag{16}$$

with $Z_0 = \sqrt{\epsilon_0/\mu_0} \sim 376.7\,\Omega$ the vacuum impedance, Q the bunch charge, σ_z the r.m.s bunch length and $\delta(\omega_z)$ the skin depth taken from Eq. (9). The function f is equal to [5]

$$f(x; x_0, y_0) \stackrel{\text{def}}{=} \frac{y_0}{y_0^2 + (x_0 - x)^2} \ . \tag{17}$$

The penetration function [5]

$$g(u) = \int_0^\infty dz\, e^{-z}\, e^{-2\,u\, z^{1/4}} \ , \tag{18}$$

is proportional to the density of ohmic power deposition $j_z^2(y)/\sigma$. Following [5], it is interesting to note that with $j_z(y) \sim \sqrt{\sigma}\exp(-y/\delta(\omega_z))$ and $\delta(\omega_z) \sim \sigma^{-1/2}$, then $j_z^2(y)/\sigma \sim \exp(-y/\delta(\omega_z))$. The power, or energy deposition at the septum $y = 0$ does not depend on the conductivity. This is visible in Eq. (16), where the y-dependence is fully contained in $g(u) = g(y/\delta(\omega_z))$, with $g(0) = 1$. Furthermore with the dependence $\delta(\omega_z) \sim \sigma^{-1/2}$, the total energy deposition by image current is proportional to $\sigma^{-1/2}$ with the consequence that somewhat poor conductors can make good spoilers as we will see later, see Section 6. The function $g(u)$ is obtained by computing the penetration depth separately for every harmonic of the bunch, contrary to the simple exponential model where the characteristic skin depth (9) is taken constant over the whole spectrum. While the two models predict the same density of energy deposition $e_d(y = 0)$ at the septum, the second one underestimates the total deposition of energy by 18% [5], a difference which is significant whenever heat diffusion is important.
The energy deposited by the passage of a Gaussian bunch writes [5]

$$E_d(x,y) = \frac{Z_0\, c}{2\pi}\, \frac{Q^2}{\pi^2\, \sigma_z^2}\, F^2(x,a) g(y/\delta(\omega_z)) \ , \tag{19}$$

where

$$F(x,a) \stackrel{\text{def}}{=} \int_{-\infty}^{+\infty} dx_0 \int_{-\infty}^{0} dy_0\, f(x, x_0, y_0)\, \rho(x_0, y_0) \ , \tag{20}$$

with f taken from Eq. (17) and the density ρ from Eq. (1). The full expansion of Eq. (20) is given in Appendix C.1 by Eq. (68). The initial map of temperature $T_{\rm ion}(x, y, t = 0) = E_d(x, y)/c_v$ is written

$$T_{\rm ion}(x, y, t = 0) = T_{0,\rm ic}\ \tilde{h}^0_x(x)\ \tilde{h}^0_y(y) \quad \text{with} \tag{21}$$

$$T_{0,\rm ic} \stackrel{\rm def}{=} \frac{Z_0\, c}{2\pi\, c_v}\, \frac{Q^2}{\pi^2\, \sigma_z^2}\, \frac{F^2(0,a)}{4\pi^2\, \sigma_x^2\, \sigma_y^2}\ , \tag{22}$$

$$\tilde{h}^0_x(x) \stackrel{\rm def}{=} F^2(x,a)/F^2(0,a) \ \text{ and} \tag{23}$$

$$\tilde{h}^0_y(y) \stackrel{\rm def}{=} g\big(y/\delta(\omega_z)\big)\ . \tag{24}$$

4.3 Black body radiation

The energy emitted by black body radiation during the passage of a train $N\delta_t$ by a surface $S = 2\,\sigma_x\, L$ writes

$$E_{\rm bb} = 2\, N\delta_t\, \sigma_x\, L \times \sigma_{\rm SB}\, T^4\ , \tag{25}$$

with $\sigma_{\rm SB} = 5.67 \times 10^{-8}$ Wm^{-2}K^{-4} the constant of Stefan-Boltzmann. The ionisation energy deposited by a train is (Section 4.1 and Table 5)

$$E_{\rm ion} = N N_e \frac{dE}{dz} L\ . \tag{26}$$

With graphite giving the largest acceptable temperature at the end of the passage of a bunch train ($T = 1900\,$K in Table 3) and with $\sigma_x \sim 10^{-4}$ m, the ratio $E_{\rm bb}/E_{\rm ion} = 4 \times 10^{-5}$ allows to neglect the black body radiation effects and to assume a perfect reflection of the heat flux at the septum.

5 Solving the heat equation

In this Section, we outline the resolution of the heat equation which is fully worked out in Appendix A. The linear differential operator to which heat diffusion obeys writes

$$\mathcal{L} = \frac{\partial^2}{\partial x_i^2} + \frac{\partial^2}{\partial y_i^2} - \frac{1}{D}\frac{\partial}{\partial t}\ , \tag{27}$$

with D the thermal diffusivity of the material assumed to be constant with the temperature, see Section 3. If the domain of application of $\mathcal{L}$ is rectangular in x and y, we can make use of the separation of variables (Appendix A.1.3). In

addition, in our case, the initial conditions are also separated (Section 4). The septum $y = 0$ is considered to be perfectly flat. Finally, we expect no substantial exchange of heat across the septum (Section 4.3). We can therefore use the principle of image source to solve the heat equation near the septum (Appendix A.2). With here a somewhat relaxed notation, the evolution with time of an initial condition expressed by a Dirac function separately for x and y, namely

$$G_0(x, t = 0) = \delta(x - x_0) \quad \text{and} \quad G_0(y, t = 0) = \delta(y - y_0) + \delta(y + y_0) \ , \tag{28}$$

writes

$$G_x(x, t) = \frac{1}{\sqrt{4\pi\, D\, t}} \exp\left(-\frac{(x - x_0)^2}{4\, D\, t}\right) \quad \text{and} \tag{29}$$

$$G_y(y, t) = \frac{1}{\sqrt{\pi\, D\, t}} \exp\left(-\frac{y + y_0^2}{4\, D\, t}\right) \cosh\left(\frac{y\, y_0}{2\, D\, t}\right) \ . \tag{30}$$

With an initial map of temperature for one bunch which is the sum of the contribution of ionisation and image current, taken respectively from Eqs. (12) and (21)

$$T(x, y, t = 0) = T_{0,\text{ion}}\, h_x^0(x)\, h_y^0(y) + T_{0,\text{ic}}\, \tilde{h}_x^0(x)\, \tilde{h}_y^0(y) \ , \tag{31}$$

the map at time t writes

$$T(x, y, t) = T_{0,\text{ion}}\, h_x(x, t)\, h_y(y, t) + T_{0,\text{ic}}\, \tilde{h}_x(x, t)\, \tilde{h}_y(y, t) \ . \tag{32}$$

with the convolution integrals

$$h_x(x, t) \stackrel{\text{def}}{=} \int_{-\infty}^{\infty} dx_0\, h_x^0(x_0)\, G(x - x_0, t) \qquad h_y(y, t) \stackrel{\text{def}}{=} \int_0^{\infty} dy_0\, h_y^0(y_0)\, G(y - y_0, t) \tag{33}$$

$$\tilde{h}_x(x, t) \stackrel{\text{def}}{=} \int_{-\infty}^{\infty} dx_0 \tilde{h}_x^0(x_0) G(x - x_0, t) \qquad \tilde{h}_y(y, t) \stackrel{\text{def}}{=} \int_0^{\infty} dy_0 \tilde{h}_y^0(y_0) G(y - y_0, t) \tag{34}$$

and the constant factors $T_{0,\text{ion}}$ and $T_{0,\text{ic}}$ taken from (13) and (22) respectively. The two functions h_x and h_y in (33) could be integrated, see Eqs. (64) and (65) in Appendix B.2. The function $\tilde{h}_y$ is reduced to the definite integral (85) in Appendix C.3. We could not reduce the function $\tilde{h}_x$ of Eq. (34) to a simple integral. To avoid using a slow 3D numerical integration, which was nevertheless made to check our calculations, we did a small approximation. The function $\tilde{h}_x^0$ is centred at $x = 0$, has an effective width larger or equal to the horizontal beam

size σ_x and is well approximated by a Gaussian function $g(x)$. Adjusting g in order to satisfy the two conditions

$$g(0) = \tilde{h}_x^0(0) \text{ and } \int_{-\infty}^{+\infty} g(x) = \int_{-\infty}^{+\infty} \tilde{h}_x^0(x) \ , \tag{35}$$

we ensure an equal initial temperature at the location of maximum heat deposition and an equal total energy deposition with both functions. In the range of σ_x where the image current heating is not negligible in comparison with the effect of ionisation (see Section 6), the diffusion of heat along the x direction is marginal, i.e. the condition $d_{\text{train}} \ll \sigma_x$ is always true. Meanwhile, as already said, the diffusion is substantial along the y direction. The maximum temperatures at the end of a train obtained with respectively the slow 3D-integration and with the fast one which uses the Gaussian approximation (Eq. 83 in Appendix C.2) differ by much less than $\delta T = 1\,\text{K}$.

5.1 Temperature map after N+1 bunches

The maximum of temperature will be reached just after the passage of the last bunch of a train, or at time $\Delta t = N\delta t$, with the first bunch passing at time $t = 0$. Using again the principle of superposition, the temperature map at time Δt is the sum of the maps computed separately for every bunch of the train. With the index n for a bunch, a time interval $t_n = (N - n)\delta t$ between this bunch and the end of the train and with using Eq (32), we get

$$T(x, y, t = \Delta t) = \sum_{n=0}^{N} \left[T_{0,\text{ion}}\, h_x(x, t_n)\, h_y(y, t_n) + T_{0,\text{ic}}\, \tilde{h}_x(x, t_n)\, \tilde{h}_y(y, t_n) \right] \ . \tag{36}$$

5.2 Computer code

In order to get the maximum excursion of temperature, it is not necessary to compute the map of temperature everywhere. With the beam centred on the axis $x = 0$, the maximum of temperature is reached along this axis. Furthermore, the density of image current is maximum at the septum and thus at $x = y = 0$ for any value of a. For $a > 0$, the contribution of ionisation is maximum at the centre of the beam $y = a$ and this maximum is independent of a. In addition, after diffusion the maximum of the distribution migrates towards the septum (see Fig. 3b). The maximum of temperature reached by summing the two processes is therefore always located at $x = y = 0$. Trial numerical calculations showed that the range inside which the impact parameter a maximises the largest temperature excursion is $-3.1\sigma_x < a < 0$. Below $a < -3.1\sigma_x$, the image current contribution decreases rapidly while the contribution of ionisation already decreases for $a < 0$. Inside the spoiler ($a > 0$) the image current decreases also rapidly with growing a values while the contribution of ionisation is nearly constant. The process of

optimisation of σ_y for a given σ_x and for the worst value of a is therefore made by evaluating Eq. (36) at $x = y = 0$ for a set a_i values in the range $-3.5\sigma_x < a_i < 0$. With our analytic approach and the use of Gauss-Legendre numerical integration the construction of the safe limit in the σ_x, σ_y plane is obtained within a few tens of minutes for a one material on a fast workstation. In order to secure our calculations and in addition to internal checks, we also computed some of the cases discussed in [5] and found very good agreement.

6 Results

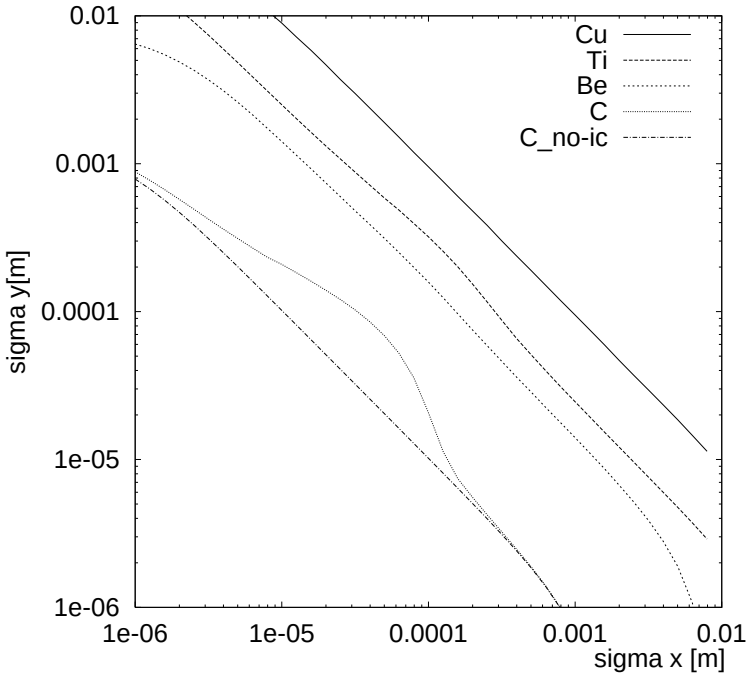

Figure 2: The boundary curve above which a full bunch train can impact the spoiler without making damage, independently of the impact parameter, with in abscissa the horizontal beam size σ_x and in ordinate the vertical one σ_y.

The curves which limit the safe area of transverse beam sizes at the spoiler are given in Fig. 2 for a few materials and for the nominal parameters of the CLIC study [3] which are given in Table 5. Aluminium and tungsten have been discarded for poor performance and to keep the figure more clear. The first obvious fact is related to the energy deposition by ionisation, which depends almost linearly on the atomic number Z, thus giving an advantage to low Z materials. On the other hand, the contribution of image current heating is weak in the case of good conductors. It is negligible with copper and slightly apparent

Table 5: Nominal bunch train parameters of the CLIC study in the 1.5 TeV beam energy option.

Parameter	Symbol	Value
Bunch population	N_e	4×10^9
Bunch charge	Q	6.408×10^{-10} C
RMS bunch length	σ_z	3×10^{-5} m
RMS bunch duration	$\sigma_t = \sigma_z/c$	10^{-13} s
Bunch spacing	δ_t	666×10^{-12} s
Number of bunches per train	$N+1$	154
Bunch train duration	$\Delta_t = N\delta_t$	1.02×10^{-7} s
Horizontal normalised emittance	$(\gamma\epsilon_x)$	68×10^{-8} rad.m
Vertical normalised emittance	$(\gamma\epsilon_y)$	2×10^{-8} rad.m
Horizontal physical emittance at $E_{\rm beam}$	ϵ_x	2.31×10^{-13} rad.m
Vertical physical emittance at $E_{\rm beam}$	ϵ_y	6.80×10^{-15} rad.m
Beam energy	$E_{\rm beam}$	1.5 TeV
Lorentz factor	$\gamma = E_{\rm beam}/m_e c^2$	2.94×10^6

with beryllium. When ionisation dominates and when the ratio of the beam sizes σ_y/σ_x is not too much different from unity, the condition $\sigma_{x,y} \gg d_{\rm train}$ applies, making the diffusion of heat marginal. The straight part of the curves is then simply explained by the factor $1/(\sigma_x\sigma_y)$ in Eq. (1). At both extremities of the plot however, with either $\sigma_{x,y} \sim d_{\rm train}$, the departure from the straight part of the curve is related to heat diffusion along either the x or the y direction. It was noted in Section 4.2 that the total energy deposition by image current is proportional to the root of the electrical resistivity, or to $\sigma^{-1/2}$. In order to show the respective contributions of ionisation and image current, we built two curves for our worst conductor, namely graphite. The curves labelled C_{no-ic} and C in Fig. 2 are obtained respectively with ionisation only and with the conductivity of Table 3. The contribution of image current heating is clearly visible. It is maximised for a large local density of beam current near the septum, i.e. with the condition $\sigma_x = \sigma_y$. On one side away from the diagonal, for large σ_x, the density of beam current falls with $1/\sigma_x$, and the density of energy deposition with $1/\sigma_x^2$. For large σ_y, the effect vanishes less rapidly. Indeed, most of the beam current dilutes away from the septum, thus the peak of the image current decreases. On the other hand, the core of the beam which stays close to the septum (the largest deposition of energy occurs for an impact parameter $a \approx -3\sigma_x$ when $\sigma_x \ll \sigma_y$), shrinks with σ_x and thus mitigates the decrease of the peak value.

6.1 Acceptable beam sizes

Considering the symmetric case $\sigma_r = \sigma_x = \sigma_y$ to simplify the discussion, the smallest safe beam sizes are $\sigma_r = 58$ μm and $\sigma_r = 125$ μm with graphite and

beryllium respectively. The corresponding values of the betatron functions at the spoiler are $\beta_{x,y} = \sigma_r^2/\epsilon_{x,y}$, where $\epsilon_{x,y}$ are the beam emittances taken from Table 5. With graphite, we get $(\beta_x, \beta_y) = (1.5 \times 10^4 \text{ m}, 5 \times 10^5 \text{ m})$ and with beryllium $(\beta_x, \beta_y) = (7 \times 10^4 \text{ m}, 2.3 \times 10^6 \text{ m})$. These values are very large. The maximum of the beta functions in the present design of the final focus of CLIC, which does not yet contain dedicated collimation sections, is $\beta_y \approx 10^6$ m. It can be concluded that graphite is a good candidate, beryllium most likely a marginal choice, while heavier metals are ruled out.

It must be stressed that these results are obtained with the data of Table 3 which are partly indicative. They must be updated for an actual variety of material while some degradation of the electrical conductivity must be expected at high frequencies, see Section 3 for a brief discussion.

7 Dielectric spoilers

The substantial difference of performance between conducting and "non-conducting graphite" ($\sigma_{r,\min} = 58$ μm and 32 μm respectively) indicates that the case of dielectric spoilers is worth studying. Produced at affordable prices by chemical vapour deposition, thin plates of diamond [13] might be a good candidate. The melting point of diamond is high (4300 K) and its mechanical properties are much better than the ones of graphite. In addition , at least up to 200 GHz, it exhibits a very marginal dielectric absorption. X.E. Lin [12] estimates its dielectric losses to be orders of magnitude smaller than the image current ohmic heating of copper up to at least 100 GHz. But two potential adverse effects must be considered. At CLIC, the r.m.s bunch length is $\sigma_z = 3 \times 10^{-5}$ m. The corresponding r.m.s. frequency is $\nu_\sigma = c/(2\pi\sigma_z) = 1.6$ THz. Dielectric losses in this frequency range must therefore be further studied. It was noted in Section 3 that similar considerations apply to metals too. The second potential problem is related to wakefield effects which, in spite of the very high beam energy, can affect the beams even in the case of small transverse offsets. These two topics are beyond the scope of this paper and require a specific study. We note that a theory of wakefield effects in a dielectric wave-guide excited by the passage of a bunch has been published recently [14].

8 Conclusions

We computed the rise of temperature after the passage of charged particles near the edge of different metallic spoilers. The deposition of heat by ionisation is smaller with low atomic number while high electrical conductivity is required to minimise image current ohmic heating. No material satisfies these two criteria. Graphite is the best candidate in spite of its poor conductivity. Our results

indicate that a low-Z insulator might be a better candidate. But wakefield adverse affects remain to be compared between metals and insulators. In both cases, some input parameters require additional care whenever a bunch length in the micrometric range is considered.

Acknowledgements

The authors wish to thank F. Caspers, C. Hauviller and J. Pett for their help and advice. They are grateful to E. Keil for a careful reading of the manuscript.

A General solution of the heat equation via the Green functions

A.1 Mathematical basis

A.1.1 Heat equation and boundary conditions

We consider an isotropic and homogeneous medium occupying an open domain V in $\mathbb{R}^N$ assumed to be finite, semi-infinite or infinite and possessing or not an interface ∂V with the vacuum. In this domain, the N-dimensional heat equation and the local flux conservation at the interface writes

$$\left\{ \begin{array}{lll} \forall\, (\mathbf{x},t) \in V \times \mathbb{R}^{+^*}\,, & [\mathcal{L}_N(T)](\mathbf{x},t) & = \; 0 \quad (\; \mathbb{R}^{+^*} \stackrel{\text{def}}{=}]\,0\,,\,+\infty[\;) \\ \forall\, (\mathbf{x},t) \in \partial V \times \mathbb{R}^{+^*}\,, & \nabla T(\mathbf{x},t) \cdot \hat{\mathbf{n}}(\mathbf{x}) & = \; 0\,, \end{array} \right. \tag{37}$$

where $\mathbf{x} \stackrel{\text{def}}{=} (x_1, \ldots, x_N)$ denotes the spatial coordinate, t the time and $\mathcal{L}_N$ the differential operator

$$\mathcal{L}_N \stackrel{\text{def}}{=} \sum_{i=1}^{N} \frac{\partial^2}{\partial x_i^2} - \frac{1}{D}\frac{\partial}{\partial t}\,, \tag{38}$$

with D [$\mathrm{m^2 s^{-1}}$] the thermal diffusivity assumed to be constant. The vector ∇T is the temperature gradient and $\hat{\mathbf{n}}(\mathbf{x})$ the unit normal vector at a given point $\mathbf{x}$ of the interface.

A.1.2 Principle of superposition

For any functions f and g which solve Eq. (37) and any parameters λ and μ, the function $\lambda f + \mu g$ fulfils the boundary condition and, due to the linearity of the operator $\mathcal{L}_N$, satisfies the heat equation:

$$\mathcal{L}_N(f) = 0 \text{ and } \mathcal{L}_N(g) = 0 \Rightarrow \mathcal{L}_N(\lambda f + \mu g) = \lambda\, \mathcal{L}_N(f) + \mu\, \mathcal{L}_N(g) = 0\,. \tag{39}$$

More generally, let us consider a real function $\omega \mapsto f(\omega)$ defined on an arbitrary parameter set Ω and a set of functions $(g_\omega)_{\omega\in\Omega}$ satisfying Eq. (37) for $t > 0$ with $(g^0_\omega)_{\omega\in\Omega}$ for initial conditions at $t = 0$:

$$g_\omega : \begin{array}{ccc} (V \cup \partial V) \times \mathbb{R}^+ & \longrightarrow & \mathbb{R} \\ (\mathbf{x},t) & \mapsto & g_\omega(\mathbf{x},t) \end{array} \text{ with } \left\{ \begin{array}{l} g_\omega(\mathbf{x},t{=}0) = g^0_\omega(\mathbf{x})\;, \quad (\mathbf{x},\omega) \in (V \cup \partial V) \times \Omega \\ [\mathcal{L}_N(g_\omega)]\,(\mathbf{x},t) = 0 \quad , \quad (\mathbf{x},t,\omega) \in V \times \mathbb{R}^{+^*} \times \Omega \\ \nabla g_\omega(\mathbf{x},t) \cdot \hat{\mathbf{n}}(\mathbf{x}) = 0\,,\; (\mathbf{x},t,\omega) \in \partial V \times \mathbb{R}^{+^*} \times \Omega\,. \end{array} \right. \tag{40}$$

Then, the function F formally defined as

$$F : \begin{array}{ccc} (V \cup \partial V) \times \mathbb{R}^+ & \longrightarrow & \mathbb{R} \\ (\mathbf{x},t) & \mapsto & F(\mathbf{x},t) \stackrel{\text{def}}{=} \displaystyle\int_\Omega d\omega\, f(\omega)\, g_\omega(\mathbf{x},t) \end{array} \tag{41}$$

solves Eq. (37) with the initial condition

$$\forall\, \mathbf{x} \in V \cup \partial V\,,\; F(\mathbf{x}, t{=}0) = \int_\Omega d\omega\, f(\omega)\, g^0_\omega(\mathbf{x})\,. \tag{42}$$

A.1.3 Separation of variables

Let us consider N functions $(f_i)_{1\leq i\leq N}$, each satisfying the one-dimensional heat equation on an open domain $V_i \subset \mathbb{R}$:

$$\begin{array}{rccc} f_i\,: & V_i \cup \partial V_i \times \mathbb{R}^+ & \longrightarrow & \mathbb{R} \\ & (x_i, t) & \mapsto & f_i(x_i, t) \end{array} \quad \text{with} \quad \mathcal{L}_1(f_i) \stackrel{\text{def}}{=} \frac{\partial^2 f_i}{\partial x_i^2} - \frac{1}{D}\frac{\partial f_i}{\partial t} = 0\,,\; 1 \leq i \leq N\,, \tag{43}$$

and let us introduce the product function F defined as

$$\begin{array}{rccc} F\,: & (V \cup \partial V) \times \mathbb{R}^+ \stackrel{\text{def}}{=} (V_1 \cup \partial V_1) \times \ldots \times (V_N \cup \partial V_N) \times \mathbb{R}^+ & \longrightarrow & \mathbb{R} \\ & (\mathbf{x}, t) \stackrel{\text{def}}{=} (x_1 \ldots x_N, t) & \mapsto & F(\mathbf{x}, t) \stackrel{\text{def}}{=} \displaystyle\prod_{i=1}^N f_i(x_i, t)\,. \end{array} \tag{44}$$

Then, by applying the relation

$$\forall\, (\mathbf{x}, t) \in V \times \mathbb{R}^{+^*}\,,\; [\mathcal{L}_N(F)](\mathbf{x}, t) \equiv \sum_{i=1}^N \left\{ \prod_{j\neq i} f_j(x_j, t)\, [\mathcal{L}_1(f_i)](x_i, t) \right\}\,, \tag{45}$$

it is clear that the function F satisfies the N-dimensional heat equation on the domain V.

A.2 Green functions

A.2.1 Definitions and notations

Let V be an open domain of $\mathbb{R}^N$ and $\mathbf{x_0}$ a point in V. The Green function $G^V_{\mathbf{x_0}}$ is defined as being the solution of Eq. (37) on V with the initial condition

$$\forall\, (\mathbf{x}, \mathbf{x_0}) \in (V \cup \partial V) \times V\,,\; G^V_{\mathbf{x_0}}(\mathbf{x}, t{=}0) = \delta(\mathbf{x} - \mathbf{x_0})\,. \tag{46}$$

Here, the N-dimensional Dirac functions $(\mathbf{x} \mapsto \delta(\mathbf{x} - \mathbf{x_0}))_{\mathbf{x_0}\in V}$ and the Green functions $(G^V_{\mathbf{x_0}})_{\mathbf{x_0}\in V}$ play the role of the initial conditions $(g^0_\omega)_{\omega\in\Omega}$ and that of the functions $(g_\omega)_{\omega\in\Omega}$ introduced in Eq. (40).

A.2.2 General solution of the heat equation via the Green functions

The usefulness of the Green functions is obvious when writing the relation

$$\forall\, \mathbf{x} \in V\ ,\ f(\mathbf{x}) = \int_V d\mathbf{x_0}\, f(\mathbf{x_0})\, \delta(\mathbf{x} - \mathbf{x_0}) \equiv \int_V d\mathbf{x_0}\, f(\mathbf{x_0})\, G^V_{\mathbf{x_0}}(\mathbf{x}, t = 0) \tag{47}$$

which stands for an arbitrary function $\mathbf{x} \mapsto f(\mathbf{x})$ defined on the domain V. This equation is similar to Eq. (42), where the parameter set Ω is the domain V itself and where the function f must be interpreted as an initial condition of a function $F(\mathbf{x}, t)$ which solves the heat equation for $t > 0$.
In other words, by using the superposition principle, for any initial condition defined on a domain V in $\mathbb{R}^N$, the solution of the N-dimensional heat equation is given by

$$F(\mathbf{x}, t) = \int_V d\mathbf{x_0}\, f(\mathbf{x_0})\, G^V_{\mathbf{x_0}}(\mathbf{x}, t)\,. \tag{48}$$

A.2.3 Green functions $G^V_{\mathbf{x_0}}$ for $V = \mathbb{R}^N$

When the domain V is the whole space $\mathbb{R}^N$, the invariance by translation of the operator $\mathcal{L}_N$ yields

$$\forall\, (\mathbf{x}, \mathbf{x_0}, t) \in \mathbb{R}^N \times \mathbb{R}^N \times \mathbb{R}^+\ ,\ G^{\mathbb{R}^N}_{\mathbf{x_0}}(\mathbf{x}, t) = G^{\mathbb{R}^N}_{\mathbf{0}}(\mathbf{x} - \mathbf{x_0}, t)\,, \tag{49}$$

where $\mathbf{0}$ denotes the null vector of $\mathbb{R}^N$. Then, using Eq. (44) and the relation

$$\delta(\mathbf{x}) = \prod_{i=1}^{N} \delta(x_i)\ ,\ \mathbf{x} = (x_1, \ldots, x_N) \in \mathbb{R}^N\,, \tag{50}$$

we obtain

$$G^{\mathbb{R}^N}_{\mathbf{x_0}}(\mathbf{x}, t) = \prod_{i=1}^{N} G^{\mathbb{R}}_0\left(x_i - x_{0_i}, t\right)\ . \tag{51}$$

The one-dimensional Green function $G^{\mathbb{R}}_0$ is searched as

$$G^{\mathbb{R}}_0(x, t) = \int_{-\infty}^{\infty} d\omega\, g(\omega, t)\, e^{i\omega x}\,, \tag{52}$$

$$\text{with } \left\{ \begin{array}{l} G^{\mathbb{R}}_0(x, 0) \overset{\text{def}}{=} \delta(x) = \dfrac{1}{2\pi} \displaystyle\int_{-\infty}^{\infty} d\omega\, e^{i\omega x} \Rightarrow \forall\, \omega \in \mathbb{R}\,,\ g(\omega, 0) = \dfrac{1}{2\pi} \\ \mathcal{L}_1\big(G^{\mathbb{R}}_0\big) = 0 \Rightarrow \partial_t g + D\,\omega^2\, g = 0 \Rightarrow g(\omega, t) = \dfrac{1}{2\pi}\, \exp(-D\,\omega^2\, t) \end{array} \right. \tag{53}$$

leading to

$$G_0^{\mathbb{R}}(x,t) = \frac{1}{\sqrt{4\pi\, D\, t}}\, \exp\left(-\frac{x^2}{4\, D\, t}\right) . \tag{54}$$

Finally, Eq. (51) yields

$$\forall\, (\mathbf{x},t) \in \mathbb{R}^N \times \mathbb{R}^{+^*}\, ,\, G_{\mathbf{x_0}}^{\mathbb{R}^N}(\mathbf{x},t) = \frac{1}{(4\pi\, D\, t)^{\frac{N}{2}}}\, \exp\left(-\frac{|\mathbf{x}-\mathbf{x_0}|^2}{4\, D\, t}\right) . \tag{55}$$

A.2.4 Green functions $G_{\mathbf{x_0}}^V$ for $V = \mathbb{R} \times \mathbb{R}^{+^*}$

In the case of a semi-infinite domain like $\mathbb{R}^{+^*} = \{y \in \mathbb{R} \,/\, y > 0\}$, the computation is a bit more tricky since the domain itself is not invariant by translation and since the Green functions must also satisfy some boundary condition at the interface, which for $\mathbb{R}^{+^*}$, write (see Eq. 37)

$$\forall\, (y_0,t) \in \mathbb{R}^{+^*} \times \mathbb{R}^{+^*}\, ,\, \left(\frac{\partial G_{y_0}^{\mathbb{R}^{+^*}}}{\partial y}\right)(y=0,t) = 0\, . \tag{56}$$

To solve this problem, it is sufficient to note that for any function f satisfying the heat equation on $\mathbb{R}$, the function $(y,t) \mapsto \tilde{f}(y,t) \stackrel{\text{def}}{=} f(-y,t)$ is also solution. As a result, the sum function $(f+\tilde{f})$ (more precisely its restriction to $y \in \mathbb{R}^+$) solves the heat equation on $\mathbb{R}^{+^*}$ while satisfying to the boundary condition (37). For any $y_0 > 0$, this result can be applied to the particular case where $f = G_{y_0}^{\mathbb{R}}$. Moreover, at time $t = 0$, the restriction to $\mathbb{R}^+$ of the function $f + \tilde{f}$ is given in this case by

$$\begin{aligned} G_{y_0}^{\mathbb{R}}(y,0) + G_{y_0}^{\mathbb{R}}(-y,0) &\equiv \delta(y-y_0) + \delta(y+y_0) = \delta(y-y_0) \\ &\equiv G_{y_0}^{\mathbb{R}^{+^*}}(y,0) \ \text{ which stands for } \ (y,y_0) \in \mathbb{R}^+ \times \mathbb{R}^{+^*}\, . \end{aligned} \tag{57}$$

The Green function $G_{y_0}^{\mathbb{R}^{+^*}}$ is then simply given by

$$\begin{aligned} G_{y_0}^{\mathbb{R}^{+^*}}(y,t) &= G_{y_0}^{\mathbb{R}}(y,t) + G_{y_0}^{\mathbb{R}}(-y,t) = G_0^{\mathbb{R}}(y-y_0,t) + G_0^{\mathbb{R}}(y+y_0,t) \\ &= \frac{1}{\sqrt{\pi\, D\, t}}\, \exp\left(-\frac{y+y_0^2}{4\, D\, t}\right)\, \cosh\left(\frac{y\, y_0}{2\, D\, t}\right) , \end{aligned} \tag{58}$$

with $G_0^{\mathbb{R}}$ derived form Eq. (54).
Finally, the Green function $G_{(x_0,y_0)}^{\mathbb{R}\times\mathbb{R}^{+^*}}$ is deduced from Eq. (44):

$$\begin{aligned} &\forall (x,y,x_0,y_0,t) \in \mathbb{R} \times \mathbb{R}^+ \times \mathbb{R} \times \mathbb{R}^{+^*} \times \mathbb{R}^{+^*} \\ &\quad G_{(x_0,y_0)}^{\mathbb{R}\times\mathbb{R}^{+^*}}(x,y,t) = G_{x_0}^{\mathbb{R}}(x,t) \times G_{y_0}^{\mathbb{R}^{+^*}}(y,t) \\ &\qquad\qquad = \frac{1}{2\pi\, D\, t}\, \exp\left(-\frac{(x-x_0)^2}{4\, D\, t}\right)\, \exp\left(-\frac{y+y_0^2}{4\, D\, t}\right)\, \cosh\left(\frac{y\, y_0}{2\, D\, t}\right) . \end{aligned} \tag{59}$$

B Solution of the heat equation with Gaussian initial conditions

B.1 Infinite medium

Let us come back to the case $V = \mathbb{R}^N$ and search a solution of the heat equation with an N-dimensional Gaussian as initial condition:

$$T(\mathbf{x}, t{=}0) = T_0 \prod_{i=1}^{N} \exp\left(-\frac{x_i^2}{2\,\sigma_i^2}\right)\,,\ \mathbf{x} = (x_1, \ldots, x_N) \in \mathbb{R}^N\,. \tag{60}$$

Thanks to Appendix A (Eq.'s 48 and 55) and after some algebra, the evolution with time of the temperature is given by

$$T(\mathbf{x}, t) \;=\; \int_{\mathbb{R}^N} d\mathbf{x_0}\, T(\mathbf{x_0}, 0)\, G_{\mathbf{x_0}}^{\mathbb{R}^N}(\mathbf{x}, t) \;=\; T_0 \prod_{i=1}^{N} \left[\frac{\sigma_i}{\sqrt{2\,D\,t + \sigma_i^2}} \times \exp\left(-\frac{x_i^2}{2}\,\frac{1}{2\,D\,t + \sigma_i^2}\right)\right]\,. \tag{61}$$

B.2 Semi-infinite medium

The case $V = \mathbb{R} \times \mathbb{R}^{+^*}$ is now considered. It corresponds to the case of a beam impacting near the edge of a collimator at time $t = 0$. The Gaussian bunch is centred in $(x = 0, y = a)$, with a negative when the bunch centroid is outside the collimator. The collimator is infinite in the x direction and semi-infinite in the y one (see Fig. 1). Assuming that the initial temperature distribution in the collimator is directly proportional to the bunch charge distribution (energy deposition by ionisation),

$$T(x, y, t{=}0) = T_0 \exp\left(-\frac{x^2}{2\sigma_x^2} - \frac{(y-a)^2}{2\sigma_y^2}\right)\,,\ x \in \mathbb{R},\ y \geq 0, \tag{62}$$

the evolution with time of the temperature can be computed using Eq.'s (48) and (59):

$$T(x, y, t) = \int_{-\infty}^{\infty} dx_0\ G_{x_0}^{\mathbb{R}}(x, t) \int_0^{\infty} dy_0\ G_{y_0}^{\mathbb{R}^{+^*}}(y, t)\ T(x_0, y_0, 0) \stackrel{\text{def}}{=} T_0 \times h_x(x, t) \times h_y(y, t)\,. \tag{63}$$

With $G_{x_0}^{\mathbb{R}}$ and $G_{y_0}^{\mathbb{R}^{+^*}}$ deduced from Eq.'s (55) and (58) respectively, and after some algebra, we get

$$h_x(x, t) \stackrel{\text{def}}{=} \int_{-\infty}^{\infty} dx_0\ G_{x_0}^{\mathbb{R}}(x, t) \exp\left(-\frac{x^2}{2\sigma_x^2}\right) = \frac{\sigma_x}{\sqrt{2\,D\,t + \sigma_x^2}} \exp\left(-\frac{x^2}{2}\,\frac{1}{2\,D\,t + \sigma_x^2}\right) \tag{64}$$

$$
\begin{aligned}
h_y(y,t) &\overset{\text{def}}{=} \int_0^\infty dy_0\; G_{y_0}^{\mathbb{R}^{+*}}(y,t)\,\exp\left[-\frac{(y-a)^2}{2\sigma_y^2}\right] \\
&= \frac{\sigma_y}{2\sqrt{2\,D\,t+\sigma_y^2}}\exp\left[-\frac{(y-a)^2}{2\,(2\,D\,t+\sigma_y^2)}\right]\left\{1+\mathrm{erf}\left[\frac{2\,a\,D\,t+y\,\sigma_y^2}{2\,\sigma_y\sqrt{D\,t\,(2\,D\,t+\sigma_y^2)}}\right]\right\}+ \\
&\quad \frac{\sigma_y}{2\sqrt{2\,D\,t+\sigma_y^2}}\exp\left[-\frac{(y+a)^2}{2\,(2\,D\,t+\sigma_y^2)}\right]\left\{1+\mathrm{erf}\left[\frac{2\,a\,D\,t-y\,\sigma_y^2}{2\,\sigma_y\sqrt{D\,t\,(2\,D\,t+\sigma_y^2)}}\right]\right\}\;,
\end{aligned}
\tag{65}
$$

with erf the standard error function given by $\mathrm{erf}(x)=\dfrac{2}{\sqrt{\pi}}\displaystyle\int_0^x dt\,e^{-t^2}$. The function f and g are plotted in Fig. 3 for different times t and assuming $a=D=\sigma_x=\sigma_y=1$. For the infinite medium (function f), the maximal temperature remains localised in $x=0$ whereas for the semi-infinite medium, the point of maximum temperature moves with time towards the interface.

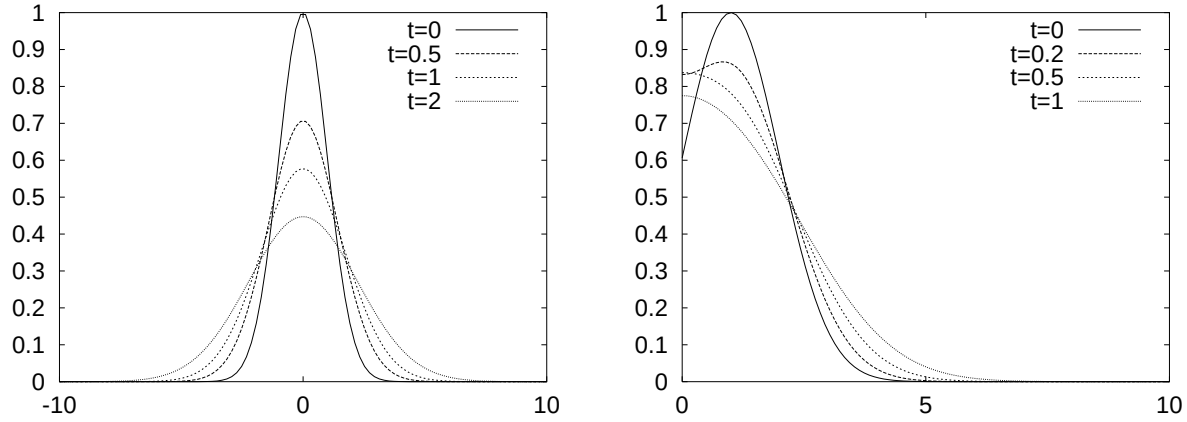

(a) Function $h_x(x,t)$ for different time t

(b) Function $h_y(y,t)$ for different time t

Figure 3: Evolution with time of the spatial temperature distribution in an infinite (Fig. a) or semi-infinite (Fig. b) medium, assuming Gaussian initial conditions

C Collimator heating induced by image current

C.1 Initial conditions

The energy deposition on the surface of a collimator induced by image current effect has been computed in [5] for a point-like bunch and is extended here to

the case of a Gaussian bunch centred at an arbitrary distance a from the septum (see Fig. 1):

$$E_d(x,y) = \frac{Z_0\, c}{2\pi} \left(\frac{Q}{\sigma_z}\right)^2 \frac{1}{\pi^2} \frac{F^2(x,a)}{4\pi^2\, \sigma_x^2\, \sigma_y^2}\, g(y/\delta) \tag{66}$$

where the notations used are defined here after:

- $\sigma_{x,y}$ are the transverse bunch sizes, σ_z the bunch length and Q the bunch charge
- a denotes the beam impact parameter (see Fig. 1) and $\delta \stackrel{\text{def}}{=} \sqrt{2/(\omega_z\, \mu_0\, \sigma)}$ is the skin depth at the characteristic bunch frequency $\omega_z = c/\sigma_z$ with σ the electrical conductivity of the material and μ_0 the permeability of the vacuum (the material is assumed to be non-magnetic).
- $Z_0 = \sqrt{\epsilon_0/\mu_0} \sim 376.7\,\Omega$ represents the vacuum impedance.
- the functions F and g are given by

$$g(u) \stackrel{\text{def}}{=} \int_0^\infty dz\, e^{-z}\, e^{-2\,u\, z^{1/4}}\,, \tag{67}$$

$$F(x,a) \stackrel{\text{def}}{=} \int_{-\infty}^{+\infty} dx_0 \int_{-\infty}^{0} dy_0\, \frac{y_0\, \exp\left(-\dfrac{x_0^2}{2\,\sigma_x^2}\right) \exp\left(-\dfrac{(y_0-a)^2}{2\,\sigma_y^2}\right)}{y_0^2 + (x_0 - x)^2}\,. \tag{68}$$

Finally, if c_v [$\mathrm{Jm^{-3}K^{-1}}$] denotes the specific heat of the material per unit volume, the initial temperature distribution is given by

$$T(x,y,t{=}0) = \frac{E_d(x,y)}{c_v} = T_{0,\mathrm{ic}} \times \frac{F^2(x,a)}{F^2(0,a)} \times g(y/\delta) \;\text{ with }\; T_{0,\mathrm{ic}} \stackrel{\text{def}}{=} \frac{Z_0\, c}{2\pi\, c_v} \frac{Q^2}{\pi^2\, \sigma_z^2} \frac{F^2(0,a)}{4\pi^2\, \sigma_x^2\, \sigma_y^2}\,. \tag{69}$$

C.2 Evolution with time of the distribution $F^2(x,a)/F^2(0,a)$

According to Eq. 48, the evolution with time of the distribution $F^2(x,a)/F^2(0,a)$ is given by

$$\tilde{h}_x(x,t) = \frac{1}{F^2(0,a)} \int_{-\infty}^{\infty} dx_0\; F^2(x_0,a)\, G^{\mathbb{R}}_{x_0}(x,t)\,, \tag{70}$$

with the Green function $G^{\mathbb{R}}_{x_0}$ and the function $F(x,a)$ defined in Eq.'s (55) and (68) respectively. In order to simplify the computations, the distribution

$F^2(x,a)/F^2(0,a)$ can be well approximated by a Gaussian function noted $\tilde{h}_x^0$ (see Fig. 4) and defined in the following way:

$$\tilde{h}_x^0(x) \stackrel{\text{def}}{=} \tilde{h}_x(x,0) = \exp\left(-\frac{x^2}{2\,\sigma_x^{(eq)^2}}\right) \text{ with } \sigma_x^{(eq)} \stackrel{\text{def}}{=} \frac{1}{\sqrt{2\pi}\,F^2(0,a)} \int_{-\infty}^{\infty} dx\, F^2(x,a)\,, \tag{71}$$

ensuring that the integral over $\mathbb{R}$ of the functions $\tilde{h}_x^0(x)$ and $F^2(x,a)/F^2(0,a)$ are the same as well as their respective value at $x=0$. As a result, by using Eq. (64), the function $\tilde{h}_x(x,t)$ will be approximated by

$$\tilde{h}_x(x,t) \approx \frac{\sigma_x^{(eq)}}{\sqrt{2\,D\,t + \sigma_x^{(eq)^2}}} \exp\left(-\frac{x^2}{2}\frac{1}{2\,D\,t + \sigma_x^{(eq)^2}}\right)\,. \tag{72}$$

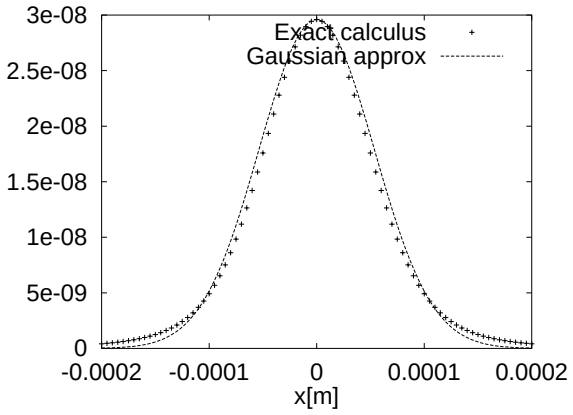

$\sigma_y = \sigma_x = 50\,\mu$m, $a = -\sigma_y$

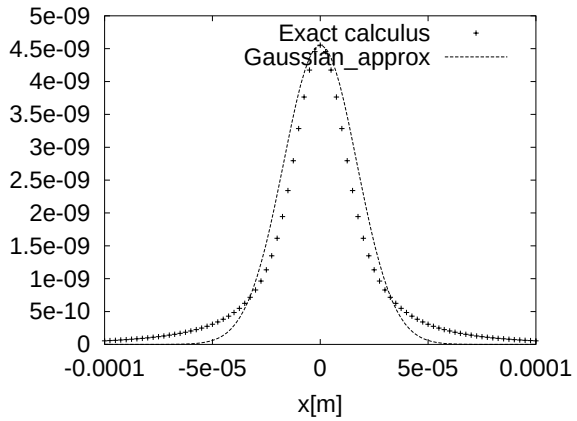

$\sigma_y = 5 \times \sigma_x = 50\,\mu$m, $a = -\sigma_y/2$

Figure 4: Comparison between the function $F^2(x,a)$ and its Gaussian approximation $F^2(0,a) \times \tilde{h}_x^0$ for different ratios σ_y/σ_x and σ_y/a

C.2.1 Computation of $F(0,a)$

The quantity $F(0,a)$ is given by (see Eq. 68)

$$F(0,a) = \int_{-\infty}^{+\infty} dx_0 \int_0^{\infty} dy_0\, \frac{y_0 \exp\left(-\frac{x_0^2}{2\,\sigma_x^2}\right) \exp\left(-\frac{(y_0+a)^2}{2\,\sigma_y^2}\right)}{y_0^2 + x_0^2}\,. \tag{73}$$

Thanks to the relation [6, p. 338],

$$\int_{-\infty}^{\infty} dx_0\, \frac{e^{-\mu^2 x_0^2}}{x_0^2 + \beta^2} = \underbrace{\text{erfc}(\beta\mu)}_{\stackrel{\text{def}}{=} 1 - \text{erf}(\beta\mu)} \frac{\pi}{\beta}\, e^{\mu^2\beta^2} \text{ for } \beta > 0\,, \tag{74}$$

the integration over the x_0 variable can be easily done leading to

$$F(0,a) = \frac{\pi^{3/2}}{\sqrt{2}}\,\sigma_y \times f_1\!\left(\frac{\sigma_y}{\sigma_x},\frac{a}{\sigma_y}\right) \text{ with } f_1(\alpha,\beta) \stackrel{\text{def}}{=} \frac{2}{\sqrt{\pi}}\int_0^\infty du\ \mathrm{erfc}(\alpha u)\ e^{\alpha^2 u^2}\, e^{-(u+\beta/\sqrt{2})^2}\,. \tag{75}$$

Note that the function f_1 has been normalised so that $f_1(0,0)=1$ and that for a round beam ($\alpha=1$), an integration by parts yields

$$f_1(1,\beta) = \frac{\sqrt{2}}{\sqrt{\pi}}\,\frac{1}{\beta}\,\left(e^{-\beta^2/2} - \mathrm{erfc}(\beta/\sqrt{2})\right) \stackrel{\beta\to 0}{\sim} \frac{2}{\pi}\,. \tag{76}$$

C.2.2 Computation of $\sigma_x^{(eq)}$

According to Eq.'s (68) and (71), we are left to compute the 5-dimensional integral

$$\begin{aligned} I &\stackrel{\text{def}}{=} \int_{-\infty}^{\infty} dx\ F^2(x,a) \\ &= \int_{-\infty}^{\infty} dx \int_{\mathbb{R}^{+2}} dy_1\,dy_2 \int_{\mathbb{R}^2} dx_1\,dx_2\ \frac{y_1\,y_2\,\exp\left(-\dfrac{x_1^2+x_2^2}{2\,\sigma_x^2}\right)\,\exp\left(-\dfrac{(y_1+a)^2+(y_2+a)^2}{2\,\sigma_y^2}\right)}{\left(y_1^2+(x_1-x)^2\right)\left(y_2^2+(x_2-x)^2\right)}\,. \end{aligned} \tag{77}$$

The integration over the x variable is performed first

$$I_1 \stackrel{\text{def}}{=} \int_{-\infty}^{\infty} dx\ \frac{y_1\,y_2}{\left(y_1^2+(x_1-x)^2\right)\left(y_2^2+(x_2-x)^2\right)} = \pi\,\frac{y_1+y_2}{(y_1+y_2)^2+(x_1-x_2)^2}\,. \tag{78}$$

Then, by applying the change of variable $u_{1,2} = (x_1 \mp x_2)/\sqrt{2}$, the integration over the variables $x_{1,2}$ yields

$$\begin{aligned} I_2 &\stackrel{\text{def}}{=} \pi \int_{\mathbb{R}2} dx_1\,dx_2\ \frac{(y_1+y_2)\,\exp\left(-\dfrac{x_1^2+x_2^2}{2\,\sigma_x^2}\right)}{(y_1+y_2)^2+(x_1-x_2)^2} = \pi\int_{\mathbb{R}2} du_1\,du_2\ \frac{(y_1+y_2)\,\exp\left(-\dfrac{u_1^2+u_2^2}{2\,\sigma_x^2}\right)}{2\,u_1^2+(y_1+y_2)^2} \\ &= \pi^{3/2}\,\sigma_x\,\frac{y_1+y_2}{\sqrt{2}}\int_{-\infty}^{\infty} du_1\ \frac{e^{-u_1^2/(2\sigma_x^2)}}{u_1^2+\left(\dfrac{y_1+y_2}{\sqrt{2}}\right)^2} \stackrel{(74)}{=} \pi^{5/2}\,\sigma_x\,\mathrm{erfc}\left(\frac{y_1+y_2}{2\sigma_x}\right)\exp\left(\frac{(y_1+y_2)^2}{4\sigma_x^2}\right). \end{aligned} \tag{79}$$

The last step consists in performing the integration over the variables $y_{1,2}$. According to Eq.'s 77, 78 and 79, the integral I has been reduced to the 2-dimensional

integral

$$I = \pi^{5/2}\,\sigma_x \int_{\mathbb{R}^{+2}} dy_1\,dy_2\ \exp\left(-\frac{(y_1+a)^2+(y_2+a)^2}{2\sigma_y^2}\right)\ \mathrm{erfc}\left(\frac{y_1+y_2}{2\sigma_x}\right)\ \exp\left(\frac{(y_1+y_2)^2}{4\sigma_x^2}\right). \tag{80}$$

Let us apply the change of variable $v_{1,2} = (y_1 \pm y_2)/\sqrt{2}$. Since, the variables $y_{1,2}$ are positive numbers, the integration over the variables $v_{1,2}$ has to be done on the domain

$$\mathcal{D} = \{(v_1, v_2) \in \mathbb{R}^2 \,|\, v_1 \geq 0 \text{ and } -v_1 \leq v_2 \leq v_1\}\ .$$

This being said, the integral I can be reduced to a one-dimensional integral in the following way:

$$\begin{aligned} I &= \pi^{5/2}\,\sigma_x \int_0^{+\infty} dv_1\ \exp\left(-\frac{(v_1+\sqrt{2}a)^2}{2\sigma_y^2}\right)\ \mathrm{erfc}\left(\frac{v_1}{\sqrt{2}\sigma_x}\right)\ e^{v_1^2/(2\,\sigma_x^2)} \int_{-v_1}^{+v_1} dv_2\ e^{-v_2^2/(2\,\sigma_y^2)} \\ &= \sqrt{2}\,\pi^3\,\sigma_x\,\sigma_y \int_0^{+\infty} dv_1\ \exp\left(-\frac{(v_1+\sqrt{2}a)^2}{2\sigma_y^2}\right)\ \mathrm{erfc}\left(\frac{v_1}{\sqrt{2}\sigma_x}\right)\ e^{v_1^2/(2\,\sigma_x^2)}\,\mathrm{erf}\left(\frac{v_1}{\sqrt{2}\sigma_y}\right), \end{aligned} \tag{81}$$

which is rewritten as

$$I = \frac{\pi^{7/2}}{2}\,\sigma_x\,\sigma_y^2 \times f_2\!\left(\frac{\sigma_y}{\sigma_x}, \frac{a}{\sigma_y}\right) \text{ with } f_2(\alpha,\beta) \stackrel{\text{def}}{=} \frac{4}{\sqrt{\pi}} \int_0^{\infty} du\ \mathrm{erfc}(\alpha u)\ e^{\alpha^2 u^2}\,\mathrm{erf(u)}\ e^{-(u+\beta)^2}\ . \tag{82}$$

Note that the function f_2 has been normalised so that

$$f_2(0,0) = \frac{4}{\sqrt{\pi}} \int_0^{\infty} du\,\mathrm{erf(u)}\ e^{-u^2} = \left[\mathrm{erf}^2(u)\right]_0^{\infty} = 1\,.$$

Finally, Eq.'s (71) and (72) rewrites

$$\tilde{h}_x(x,t) \approx \frac{\sigma_x^{(eq)}}{\sqrt{2\,D\,t + \sigma_x^{(eq)^2}}}\ \exp\left(-\frac{x^2}{2}\frac{1}{2\,D\,t+\sigma_x^{(eq)^2}}\right) \text{ with } \sigma_x^{(eq)} = \frac{f_2(\sigma_y/\sigma_x, a/\sigma_y)}{f_1^2(\sigma_y/\sigma_x, a/\sigma_y)} \times \frac{\sigma_x}{\sqrt{2}}\,, \tag{83}$$

where the functions f_1 and f_2 are defined in Eq.'s (75) and (82).

C.3 Evolution with time of the distribution $g(y/\delta)$

We are still left to evaluate the function $\tilde{h}_y(y,t)$ describing the evolution with time of the distribution $g(y/\delta)$ in the semi-infinite medium $\{y \geq 0\}$. By using Eq. (48) and the definition of g (Eq. 67), we get

$$\tilde{h}_y(y,t) = \int_0^{\infty} dy_0\ g(y_0/\delta)\,G_{y_0}^{\mathbb{R}^{+*}}(y,t) = \int_0^{\infty} dz\,e^{-z} \int_0^{\infty} dy_0\ \exp\left(-2\,\frac{z^{1/4}\,y_0}{\delta}\right)\ G_{y_0}^{\mathbb{R}^{+*}}(y,t)\,. \tag{84}$$

With the Green function $G_{y_0}^{\mathbb{R}^{+*}}$ taken from Eq. (58) and after some algebra, the integration over the y_0 variable yields

$$\tilde{h}_y(y,t) = \frac{e^{-y^2/(4Dt)}}{2} \times \left\{ \int_0^\infty dz\, e^{-z}\, \exp\left[\left(\frac{2\, z^{\frac{1}{4}} \sqrt{Dt}}{\delta} - \frac{y}{2\sqrt{Dt}} \right)^2 \right] \operatorname{erfc}\left(\frac{2\, z^{\frac{1}{4}} \sqrt{Dt}}{\delta} - \frac{y}{2\sqrt{Dt}} \right) + \right.$$
$$\left. \int_0^\infty dz\, e^{-z}\, \exp\left[\left(\frac{2\, z^{\frac{1}{4}} \sqrt{Dt}}{\delta} + \frac{y}{2\sqrt{Dt}} \right)^2 \right] \operatorname{erfc}\left(\frac{2\, z^{\frac{1}{4}} \sqrt{Dt}}{\delta} + \frac{y}{2\sqrt{Dt}} \right) \right\}. \tag{85}$$

References

[1] The NLC Design Group, *Zeroth-order Design Report for the Next Linear Collider*, LBNL-Pub-5424, SLAC Report 474, UCRL-ID-124161, May 1966.

[2] *Conceptual Design of a 500 GeV* e^+e^- *Linear Collider with Integrated X-ray Laser Facility*, R.Brinkmann et al. Eds, DESY 1997-048, ECFA 1997-182, May 1997.

[3] The CLIC study team, *A 3 TeV* e^+e^- *Linear Collider based on CLIC Technology*, edited by G. Guignard, CERN 2000-008, July 2000.

[4] J.B. Jeanneret and E. Wildner, CERN SL-99-072 AP, CLIC Note 421, October 1999.

[5] X.E. Lin and D.H. Whittum, *Image current heating on metal surface due to charged bunches*, Phys. Rev. ST, Accelerators and beams, **3**, 101001 (2000).

[6] I.S. Gradshteyn and I.M. Ryzhik, *Table of integrals, series, and products* (Academic Press, 1965).

[7] *Numerical recipes in C*, Cambridge university press 1988-92, p. 147-161.

[8] *Handbook of Chemistry and Physics*, edited by R.C. Weast (CRC Press, 1974).

[9] C. Caso et al., *Review of Particle physics*, Eur. Phys. J. C3, 1 (1998).

[10] G.W.C. Kaye et al., *Tables of Physical and Chemical Constants* (Longmans Ed., 1968).

[11] K. Kikuchi, IEEE Trans. on Instrum. and Meas., **39**, N° 2, 395 (1990).

[12] X.E. Lin, *Diamond coating in Accelerator Structures*, in CP472, Advanced Acc. Concepts, 8th workshop, edited by W. Lawson, C. Bellamy and D. Brosius, The American Institute of Physics, 1999.

[13] De Beers Industrial Diamond Division, Shannon, CO. Clare, Ireland.

[14] S.Y. Park and J.L. Hirschfield, Phys. Rev. E **62**,1266 (2000).